Experimental nuclear charge density and theoretical description of the above-barrier light heavy-ion fusion process*

I. I. Gontchar[1†] M. V. Chushnyakova[2]

[1]Physics and Chemistry Department, Omsk State Transport University, Omsk, Russia
[2]Physics Department, Omsk State Technical University, Omsk, Russia

Abstract: Theoretical modeling of nucleus-nucleus collisions is often based on the nucleus-nucleus potential. One of the advanced methods for constructing this potential is the semi-microscopical double-folding model with M3Y-Paris NN-forces. Proton and neutron densities are significant components of this model. The correct nucleon density (ND) must reproduce the experimental nuclear charge density (NCD). However, those who deal with modeling the fusion process typically disregard this circumstance. We aim to achieve a good description of both the nuclear charge density and above-barrier fusion cross sections of even-even light nuclei with $Z = N$. We consider several versions of NDs available in literature and construct our own approximation for the ND of the even-even spherical nuclei ^{12}C, ^{16}O, and ^{40}Ca, abbreviated as FE-density (Fermi+exponential). We carefully compare the NCDs resulting from different versions of NDs with the experimental NCDs. After finding the nucleus-nucleus potential using the double-folding model with the density dependent M3Y-Paris NN-forces and FE densities, we evaluate the above-barrier fusion cross sections for five reactions, ^{12}C+^{12}C, ^{12}C+^{16}O, ^{16}O+^{16}O, ^{16}O+^{40}Ca, and ^{40}Ca+^{40}Ca, for which experimental data are available. The cross sections are calculated using two approaches: a) the barrier penetration model and b) the trajectory model with surface friction (TM). To find the transmission coefficients for the TM, the Langevin equations are employed. For all considered reactions, our TM typically reproduces the above-barrier experimental cross sections within 10−15%. The only adjustable parameter of the model, the optimal friction strength K_{Rm}, is found to be approximately 90 $\mathrm{zs\cdot GeV^{-1}}$ for the light reactions ^{12}C+^{12}C, ^{12}C+^{16}O, and ^{16}O+^{16}O and approximately 15 $\mathrm{zs\cdot GeV^{-1}}$ for the heavy reactions ^{16}O+^{40}Ca and ^{40}Ca+^{40}Ca. The latter findings are in reasonable agreement with the systematics found previously. Thus, the FE-recipe allows highly accurate and simultaneous reproduction of both the nuclear charge density and above-barrier fusion cross sections of five reactions involving ^{12}C, ^{16}O, and ^{40}Ca nuclei.

Keywords: nuclear charge densities, nucleon densities, heavy-ion fusion, surface friction, double-folding model

DOI: 10.1088/1674-1137/acd682

I. INTRODUCTION

Theoretical modeling of nucleus-nucleus collisions is useful because it reduces experimental labor and expenses. Moreover, this modeling enables us to understand the mechanism of nucleus-nucleus interactions. To model the fusion process of two nuclei, the time-dependent Hartree–Fock approach [1−4] is often considered one of the most advanced methods. However, there are two shortcomings of this approach: (i) it is highly computer-time consuming, and (ii) it is difficult to account for fluctuations of the nucleus shape. Therefore, in literature, simplified dynamical approaches are widely used, such as the quantum diffusion approach [5−8], coupled-channels method [9−12], and trajectory model with surface friction [13−16].

In all these simplified approaches, a crucial role is played by the nucleus-nucleus effective interaction potential, consisting of the Coulomb U_{C}, nuclear U_n, and centrifugal U_{rot} terms. The nuclear term of this potential is the least defined quantity. In many studies, this term is calculated using the semi-microscopical double folding model with frozen densities [5, 8, 17−22]. The simplest formula for this model reads as

$$U_n(R) = \int \mathrm{d}\vec{r}_1 \int \mathrm{d}\vec{r}_2 \rho_{A1}(r_1)\, \mathrm{v}_{NN}\left(\left|\vec{R} - \vec{r}_2 + \vec{r}_1\right|\right) \rho_{A2}(r_2). \tag{1}$$

Here, ρ_{A1} (ρ_{A2}) is the point nucleon projectile (target)

Received 19 February 2023; Accepted 18 May 2023; Published online 19 May 2023

* Supported by the Foundation for the Advancement of Theoretical Physics and Mathematics "BASIS."

† E-mail: vigichar@hotmail.com

©2023 Chinese Physical Society and the Institute of High Energy Physics of the Chinese Academy of Sciences and the Institute of Modern Physics of the Chinese Academy of Sciences and IOP Publishing Ltd

density, v_{NN} is the effective nucleon-nucleon interaction, $\vec{R}$ corresponds to the projectile-target center-to-center distance, and $\vec{r}_1$ and $\vec{r}_2$ are the radius-vectors of the interacting points of the projectile and target nuclei, respectively. Note that in the present study, we consider the collisions of two spherical nuclei; the nucleon density (ND) is the sum of the proton and neutron densities, $\rho_{Ai}=\rho_{Zi}+\rho_{Ni}$ $(i=1,2)$. To evaluate the Coulomb nucleus-nucleus interaction energy $U_{\rm C}(R)$, one can use Eq. (1) by appropriately changing the densities and nucleon-nucleon interaction.

The NDs $\rho_{A1(2)}$ arrive at Eq. (1) from different sources that are external with respect to the double folding approach. The problem, however, is that the NDs are not the observable quantities. Although experimental information on the neutron density was recently obtained [23, 24], the usual way to experimentally explore the interior of the nucleus is to irradiate it with electrons; thus, the measured quantity is the nuclear charge density (NCD) [25−27]. For the collision of spherical nuclei, the NCD is not considered to be of crucial importance when calculating the Coulomb term of the nucleus-nucleus potential [18]. However, for consistency, the theoretical NDs used in Eq. (1) must provide NCDs in agreement with the experimental NCDs, as it is in nature.

The idea behind the present study is to make use of experimental NCDs to obtain correct NDs, which are then implemented in the double folding potential. Three spherical even-even nuclei with $N=Z$ are employed: ^{12}C, ^{16}O, and ^{40}Ca. Although there is some experimental information on the deformed shape of ^{12}C (see, for example, [28, 29] and references therein), this nucleus is considered a spherical one in many studies [14, 20, 21, 30, 31]. Moreover, it is well established that at above barrier collision energies, structure effects, such as nuclear deformation, do not significantly manifest themselves [32]. Therefore, we believe it is a reasonable approximation to consider ^{12}C a spherical nucleus in our calculations.

In the collision of light heavy ions, the capture of reagents into the orbital motion results in their fusion into a compound nucleus. This is why we use the term "fusion" even though we only calculate capture cross sections. Following [21], we assume that $\rho_Z=\rho_N$ for these nuclei and propose a novel approach for ND parameterization. These densities are used to evaluate the above-barrier capture cross-sections of the ^{12}C+^{12}C, ^{16}O, ^{16}O+^{16}O, ^{40}Ca, and ^{40}Ca+^{40}Ca reactions.

The paper is organized as follows. In Sec. II, we discuss the relationship between the NCD and ND as well as the different versions of NDs available in literature. In Sec. III, a novel parameterization for NDs is described, and the calculated NCDs are compared with the experimental values. The models used to calculate the fusion cross sections are considered in Sec. IV. Theoretical fusion cross-sections are compared with the experimental values in Sec. V. Finally, Sec. VI presents the conclusions.

II. NUCLEAR CHARGE DENSITY AND NUCLEON DENSITY

The experimental NCDs are approximated using the sum of Gaussians (SOG) analysis [26]:

$$\rho_{q\exp}(r)=\sum_i A_i\left\{\exp\left[-\left(\frac{r-R_i}{\gamma}\right)^2\right]+\exp\left[-\left(\frac{r+R_i}{\gamma}\right)^2\right]\right\} \tag{2}$$

with

$$A_i=\frac{ZQ_i}{2\pi^{3/2}\gamma^3\left(1+2R_i^2/\gamma^2\right)}, \tag{3}$$

where

$$\sum_i Q_i=1. \tag{4}$$

The coefficients Q_i, and the positions R_i and width γ of the Gaussians are tabulated in [26].

Provided the proton density ρ_Z is known, the NCD in a spherical nucleus, $\rho_q(r)$, as a function of the distance from its center, r, can be calculated using the convolution method [33],

$$\rho_q(r)=\int {\rm d}\vec{r}_p\rho_Z\left(r_p\right)f_p\left(\left|\vec{r}-\vec{r}_p\right|\right). \tag{5}$$

Here, $\vec{r}_p$ denotes the radius-vector of the proton center of mass, and f_p is the charge distribution inside proton.

For this distribution as a function of $l=\left|\vec{r}-\vec{r}_p\right|$, we use the exponential distribution [34]

$$f_{pe}(l)=\frac{3\sqrt{(3)}}{\pi R_{pe}^3}\exp\left(-\frac{2\sqrt{3}l}{R_{qp}}\right) \tag{6}$$

where R_{qp} is the experimental value of the root mean square proton charge radius $R_{qp}=0.8783$ fm [27]. Although this value has been found to be 4% smaller in recent experiments [35, 36], in this study, we use the value from [27].

In literature, we can find several options for the NDs. In [37], theoretical densities calculated within the Hartree-Fock-Bogolubov approach are approximated using $2pF$ profiles with different radius and diffuseness

parameters for protons (Z) and neutrons (N)

$$\rho_{i2pF}(r) = \frac{\rho_{i2pFC}}{1+\exp\left[\frac{r-R_{0i2pF}}{a_{i2pF}}\right]}. \tag{7}$$

Here, $i = Z, N$, R_{0i2pF} and a_{i2pF} are the half-central density radius and diffuseness parameters, respectively, and ρ_{i2pFC} originates from the normalization condition. However, for ^{12}C, this type of density profile is absent in [37].

For ^{12}C and ^{16}O, the following Gaussian-like densities can be found in [21]:

$$\begin{aligned}\rho_{AG}(r) &= 2\rho_{NG}(r) = 2\rho_{ZG}(r)\\ &= \frac{4}{\pi^{\frac{3}{2}} s_{AG}^3}\left(1+\frac{F_{AG}r^2}{s_{AG}^2}\right)\exp\left(-\frac{r^2}{s_{AG}^2}\right)\end{aligned} \tag{8}$$

with $s_{AG} = 1.5840$ fm, $F_{AG} = 4/3$ for ^{12}C, and $s_{AG} = 1.7410$ fm, $F_{AG} = 2$ for ^{16}O. However, this type of density profile is not known to us for ^{40}Ca.

In [8], an effective analytical method for evaluating double-folding integrals was developed. For the NDs, a symmetrized Woods-Saxon function was used and applied systematically in a study by Sargsyan *et al.* [5]. In our case, this function reads as

$$\begin{aligned}\rho_{AS}(r) &= 2\rho_{NS}(r) = 2\rho_{ZS}(r)\\ &= \frac{\rho_{SC}\sinh(R_{0S}/a_S)}{\cosh(R_{0S}/a_S)+\cosh(r/a_S)}.\end{aligned} \tag{9}$$

Here, $R_{0S} = r_{0S}A^{1/3}$, r_{0S}=1.15 fm, a_A=0.53 fm for ^{12}C, ^{16}O and 0.55 fm for ^{40}Ca. We find ρ_{SC} from the normalization condition.

III. NOVEL PARAMETERIZATION FOR NUCLEON DENSITIES

We propose a novel algorithm for finding NDs based on experimental NCDs. We call it Fermi+exponential and denote it as FE:

$$\rho_{AFE}(r) = 2\rho_{ZFE}(r) = 2\rho_{NFE}(r)$$

$$= \begin{cases} \rho_{FEC}\left[1+\exp\{(r-R_{0FE})/a_{AF}\}\right]^{-1} & \text{at } r < R_{0FE}, \quad (10)\\ 0.5\rho_{FEC}\exp\{(R_{0FE}-r)/a_{AE}\} & \text{at } r \geq R_{0FE}. \quad (11)\end{cases}$$

First, we approximate the ND using the Fermi profile (Eq. (10)). The values of R_{0FE} and a_{AF} are varied to reach good agreement with the inner part of the experimental NCD. Then, for $r \geq R_{0FE}$, the ND is approximated by an exponential function (Eq. (11)). At $r = R_{0FE}$, Eqs. (10) and (11) result in $0.5\rho_{FEC}$. The diffuseness of the exponential tail, a_{AE}, is varied to fit the tail of the NCD, and then the constant ρ_{FEC} is found from the normalization condition

$$A = \int d\vec{r}\,\rho_{AFE}(r). \tag{12}$$

The parameters R_{0FE}, a_{AF}, and a_{AE} providing the best agreement with the experimental NCDs are presented in Table 1.

The NCDs resulting from $\rho_{AS}(r)$, $\rho_{AG}(r)$, and $\rho_{Z2pF}(r)$ (that is, $\rho_{qS}(r)$, $\rho_{qG}(r)$, and $\rho_{q2pF}(r)$) as well as from the novel algorithm (FE algorithm henceforth $\rho_{qFE}(r)$) are compared with the experimental NCDs in Figs. 1, 2, and 3 for ^{12}C, ^{16}O, and ^{40}Ca, respectively. For the ^{12}C and ^{16}O nuclei, the Gaussian ND-profile results in good agreement with $\rho_{q\exp}(r)$ in the nuclear interior, whereas for the tail, $\rho_{qG}(r)$ underestimates the data. The FE-algorithm provides somewhat poorer agreement with $\rho_{q\exp}(r)$ in the interior but a considerably better reproduction of the data in the tail. The NDs $\rho_{qS}(r)$ disagree with $\rho_{q\exp}(r)$ for all values of r.

For ^{40}Ca (see Fig. 3), the Gaussian ND profile is absent, and we compare $\rho_{q\exp}(r)$ with the charge density resulting from the 2pF ND instead. The charge densities $\rho_{q2pF}(r)$ and $\rho_{qFE}(r)$ are in good agreement with each other. For the interior, they reproduce $\rho_{q\exp}(r)$ well, whereas for the tail, the agreement worsens. $\rho_{qS}(r)$ again significantly deviates from the data.

For a quantitative measure of the agreement between

Table 1. Experimental rms charge radii $r_{q\exp}$ with their errors [27], the fractional differences for the radii ξ_{rG}, ξ_{r2pF}, ξ_{rS}, and ξ_{rFE}, the average differences in the densities $\xi_{\rho G}$, $\xi_{\rho 2pF}$, $\xi_{\rho S}$, and $\xi_{\rho FE}$, the parameters resulting from the FE algorithm, R_{0FE}, a_{AF}, and a_{AE}, and the energy of the second excited state, E_2.

Nucleus	$r_{q\exp}$ /fm	exp err /fm	ξ_{rG} (%)	ξ_{r2pF} (%)	ξ_{rS} (%)	ξ_{rFE} (%)	$\xi_{\rho G}$ (%)	$\xi_{\rho 2pF}$ (%)	$\xi_{\rho S}$ (%)	$\xi_{\rho FE}$ (%)	R_{0FE} /fm	a_{AF} /fm	a_{AE} /fm	E_2 /MeV
^{12}C	2.4702	0.0022	0.9	n/a	19.9	-0.3	21.3	n/a	371	11.0	2.50	0.27	0.42	7.7
^{16}O	2.6991	0.0052	2.0	n/a	14.9	1.6	18.4	n/a	129	7.9	2.80	0.25	0.47	6.1
^{40}Ca	3.4778	0.0012	n/a	0.8	8.4	-0.5	n/a	18.3	55.2	12.7	3.75	0.62	0.54	3.7

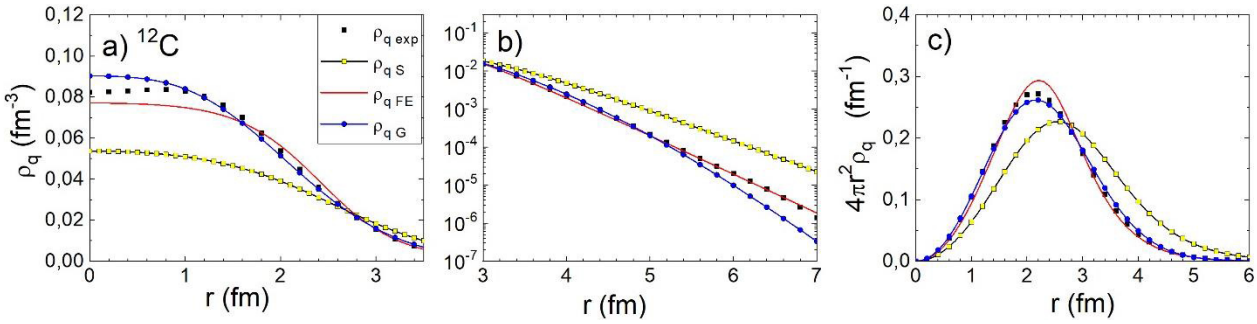

Fig. 1. (color online) Nucleus charge densities in linear (a) and logarithmic (b) scales and the "radial" charge density $4\pi r^2\rho_q(r)$ (c) for ^{12}C. The black squares (see Eq. (2)) indicate the experimental density, the light squares represent Sargsyan density, the lines without symbols denote FE densities, and the lines with solid circles represent Gaussian density.

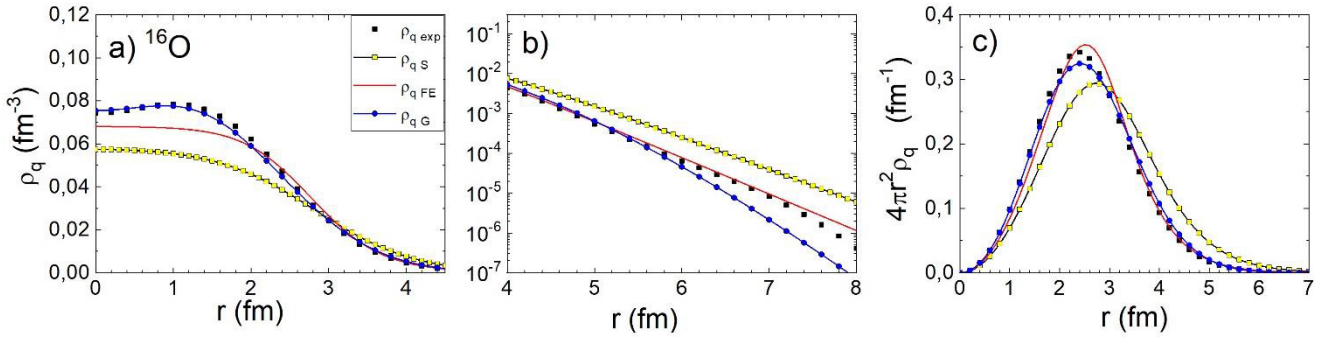

Fig. 2. (color online) Same as in Fig. 1 but for ^{16}O.

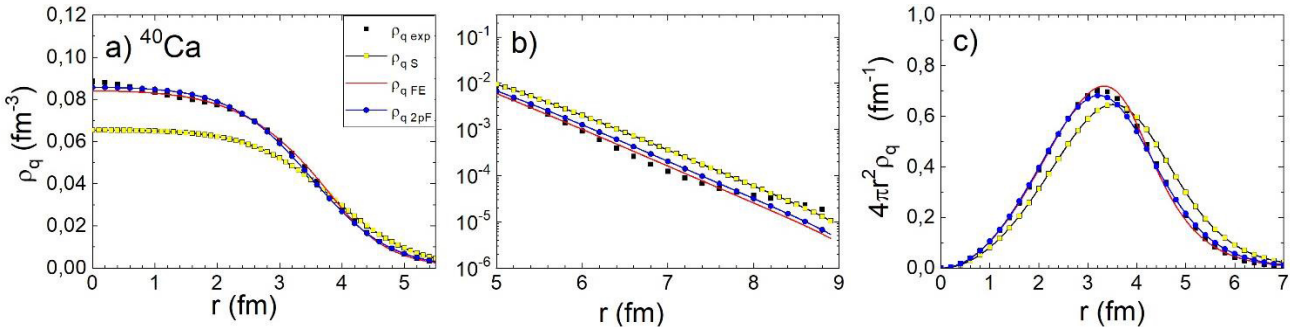

Fig. 3. (color online) Same as in Figs. 1, 2 but for ^{40}Ca. The lines with solid circles represent 2pF density.

the theoretical and experimental NCDs, we use two quantities. The first, the fractional difference between the root mean square radii, ξ_{ru}, reads as

$$\xi_{ru} = r_{qu}/r_{q\,\mathrm{exp}} - 1. \tag{13}$$

The second quantity is the average fractional difference between the NCDs, $\xi_{\rho u}$:

$$\xi_{\rho u} = \frac{1}{Q}\sum_{i=1}^{Q}\left|1 - \frac{\rho_{qu}(r_i)}{\rho_{q\mathrm{exp}}(r_i)}\right|. \tag{14}$$

Here, the summation is limited by the range of the experimental NCDs [26]. In Eqs. (13) and (14), $u = G$, FE, $2pF$, or S.

The results of the quantitative comparison are presented in Table 1. We can see that for the NCD, the FE algorithm provides significantly better agreement with the experimental values than the others NDs. Yet, the deviation ρ_{qS} from the experimental NCDs is the most striking.

IV. MODELS FOR FUSION CROSS SECTIONS

Of the four considered versions of the densities, only $\rho_{AS}(r)$ and $\rho_{AFE}(r)$ are available for the nuclei ^{12}C, ^{16}O, and ^{40}Ca. However, the NDs $\rho_{AS}(r)$ of Refs. [5, 8, 19] fail to produce charge densities in agreement with experimental values. Moreover, in those studies, Migdal Skyrme-type *NN* forces were used. Therefore, for the re-

mainder of the paper, all calculations are performed with only FE-densities. Here, we provide only a brief description of the options employed; all the details on the version of the double-folding model utilized in the this study can be found in [13, 15].

The potential energies for the reactions under consideration are calculated within the framework of the double folding model (see Eq. (1)) with the frozen densities $\rho_{AFE}(r)$. For the effective nucleon-nucleon forces, v_{NN}, the M3Y-Paris parameterization is applied. The nuclear term of the nucleus-nucleus potential consists of direct and exchange parts. For the latter, the option with finite range *NN*-forces is employed. Both direct and exchange parts are density dependent. There are approximately ten parameterizations of this dependence [21, 31]; we use the DD2-option according to Table 2 of Ref. [38]. It is known in literature that the version with the finite-range exchange term and this density dependence of v_{NN} successfully reproduces the nuclear matter equilibrium density, binding energy, and incompressibility as well as the high precision above-barrier fusion heavy-ion cross-sections.

Information on the reactions under consideration is presented in Table 2. For the reactions ^{12}C +^{12}C, ^{16}O and ^{16}O +^{16}O, ^{40}Ca, the calculated *s*-wave barrier energies B_0 are in good agreement with the experimental values. For the reaction ^{40}Ca+^{40}Ca, the agreement is somewhat worse. However, one should remember that the "experimental barrier energy" is based on not only the measured fusion cross sections but also the model used for the analysis of these cross sections.

In the present study, the capture cross-sections are calculated using standard quantum mechanical formulas (see, for example, [39], Eqs. (1.38) and (1.143)):

$$\sigma_{\rm th} = \frac{\pi\hbar^2}{2m_R E_{\rm c.m.}} \sum_{L=0,1,2,...}^{L_{\max}} (2L+1)T_L \tag{15}$$

for the ^{12}C+^{16}O and ^{16}O+^{40}Ca reactions, and

$$\sigma_{\rm th} = \frac{\pi\hbar^2}{m_R E_{\rm c.m.}} \sum_{L=0,2,4...}^{L_{\max}} (2L+1)T_L. \tag{16}$$

for the other reactions. Here, $E_{\rm c.m.}$ is the collision energy in the center-of-mass frame, $m_R = m_n A_1 A_2/(A_1+A_2)$, L denotes the angular momentum in units of $\hbar$, $L_{\max}$ is the maximal angular momentum above which the transmission coefficient equals zero, and m_n represents the nucleon mass.

In this study, the transmission coefficients are evaluated using two options. In the first, the barrier penetration model (BPM) within the framework of the parabolic approximation is applied:

$$T_{L\rm BPM} = \left\{1+\exp[2\pi(U_{bL}-E_{\rm c.m.})/(\hbar\Omega_{bL})]\right\}^{-1}. \tag{17}$$

Here, U_{bL} and $\Omega_{bL} = \sqrt{C_{2bL}/m_q}$ denote the barrier height and curvature calculated for the L-th partial wave (see definition of m_q below). The cross-sections evaluated using this option are denoted as $\sigma_{\rm BPM}$. They approximately correspond to the upper limit of the theoretical cross-sections $\sigma_{\rm th}$ obtained dynamically because accounting for dissipation inhibits the fusion process.

The second option for obtaining the transmission coefficient is the trajectory model with surface friction (TM) [13, 49]. The physical picture of the TM is similar to that in Ref. [50]. An imaginary Brownian particle with

Table 2. For the five reactions under consideration, the following quantities are presented: the *s*-wave barrier radius R_{b0} and width $\hbar\Omega_{b0}$, B_Z (see Eq. (23)), the *s*-wave barrier heights B_0 calculated in this study, the *s*-wave experimental barrier height $B_{0\rm exp}$ (with its error) and the corresponding references, the references to the experimental cross sections, the value $E_{\rm cut}$ discussed in Sec. V, the number of data points used for the detailed quantitative analysis υ, the friction strength K_{Rm} (with its error) providing the least value of χ^2, χ^2_m (see Eq. (21)), and $E_{\rm cut} = B_0 + E_2$.

Reaction	R_{b0} /fm	$\hbar\Omega_{b0}$ /MeV	B_Z /MeV	B_0 /MeV	B_{0exp}(err) /MeV	Source of $B_{0\rm exp}$	Source of $\sigma_{\rm exp}$	E_{cut} /MeV	υ	K_{Rm}(err) /(zs·GeV^{-1})	χ^2_m
R1 ^{12}C+^{12}C	7.73	2.17	7.87	6.22	5.8(0.3)	[40]	[41]	13.9	27	77(7)	2.8
R1 ^{12}C+^{12}C	–	–	–	–	6.17(0.10)	[42]	[40]	–	45	88(10)	2.9
R2 ^{12}C+^{16}O	8.12	2.15	9.99	7.90	7.7(0.4)	[41]	[41]	14.0	25	85(10)	1.6
R2 ^{12}C+^{16}O	–	–	–	–	7.69(0.10)	[43]	–	–	–	–	–
R3 ^{16}O+^{16}O	7.99	2.33	12.71	10.72	11.2(0.6)	[41]	[44]	16.8	48	44(8)	7.1
R4 ^{16}O +^{40}Ca	9.29	2.46	26.97	23.04	23.7(1.0)	[45]	[45,46]	26.7	3+6	18(7)	0.4
R5 ^{40}Ca +^{40}Ca	10.04	2.55	58.55	53.30	50.6(2.8)	[41]	[47]	57.0	4	13(11)	0.9
R5 ^{40}Ca +^{40}Ca	–	–	–	–	51.5(0.5)	[48]	[48]	–	11	7(6)	2.5

reduced mass, whose motion corresponds to the relative motion of the colliding nuclei, wanders, influenced by conservative, dissipative, and random (fluctuating) forces. In this study, only the collisions at energies well exceeding the Coulomb barrier are considered. Therefore, tunneling and channel coupling can be safely neglected.

The motion of the Brownian particle is described by a dimensionless coordinate q, which is proportional to the distance between the centers of the colliding nuclei R. In [49], it was demonstrated that the orbital degree of freedom can be ignored because it influences the cross-sections within the framework of the statistical errors (typically 1%). In [51], it was proved that in the collision process, memory effects at distances larger than the contact configuration can be discarded. Because this configuration is never reached in our modeling, we use stochastic Langevin-type equations with white noise and instant dissipation:

$$\mathrm{d}p = \left\{ -\frac{\mathrm{d}U_{\rm tot}}{\mathrm{d}q} + \frac{\hbar^2 L^2}{m_q q^3} - \frac{p}{m_q} K_R \left[\frac{\mathrm{d}U_n}{\mathrm{d}q} \right]^2 \right\} \mathrm{d}t + \left| \frac{\mathrm{d}U_n}{\mathrm{d}q} \right| \mathrm{d}W \sqrt{2\theta K_R}, \tag{18}$$

$$\mathrm{d}q = \frac{p\mathrm{d}t}{m_q}. \tag{19}$$

Here, $U_{\rm tot} = U_n + U_{\rm C}$ denotes the total nucleus-nucleus interaction energy, p denotes the linear momentum corresponding to the relative motion of the colliding nuclei, $\hbar L$ is the projection of the orbital angular momentum onto the axis perpendicular to the reaction plane, K_R denotes the dissipation strength coefficient, and θ represents the thermal energy (temperature). The quantity m_q is the inertia parameter

$$m_q = m_R R_{PT}^2 \tag{20}$$

where $R_{PT} = 1.2\left(A_1^{1/3} + A_2^{1/3}\right)$ fm. In fact, the model is designed in such a way that its physical results are independent of the real value of R_{PT}. The time-dependent temperature θ in Eq. (18) is related to the dissipated energy via the Fermi-gas relation. All details on how θ is evaluated can be found in Refs. [13, 49].

The dissipative force (the final term in the figure brackets in Eq. (18)) is related to the nuclear term of the interaction energy via the surface friction expression [50, 52]. The random force (the final term in Eq. (18)) is proportional to the increment of the Wiener process $\mathrm{d}W$, which possesses zero average and a variance equal to $\mathrm{d}t$. Eqs. (18) and (19) are solved numerically using the Runge-Kutta method (find details in [49, 53]).

Within the framework of the TM, the transmission coefficient T_{LTM} is defined as the number of captured trajectories divided by the total number of trajectories for each L-value. The capture conditions are described in Sec. II F of Ref. [49]. More details on the TM are presented in Refs. [13, 54].

V. COMPARISON OF THE CROSS SECTIONS WITH THE EXPERIMENT

In Fig. 4, we show nearly all the above-barrier experimental fusion cross sections $\sigma_{\rm exp}$ found in literature. For reaction R1 (panel a), five sets of data are available [40, 41, 43, 55, 56]. Keeping in mind that sub- and near-barrier data cannot be used in our study, we exclude the data of Refs. [57−59]. We also omit the data from Refs. [42, 60] because there are only several convenient points in each of these articles, and the experimental errors are rather large. The data in Fig. 4(a) form two blocks: those from Refs. [40, 55] and those from Refs. [41, 43, 56]. Inside each block, the data agree with each other, whereas there seems to be some disagreement between the data of different blocks. Therefore, we select the data from [40] and [41] for detailed quantitative separate comparison with the calculations.

A similar problem seems to arise for reaction R3 (see Fig. 4(c)). However, three datasets [41, 44, 62] are in reasonable agreement with each other. Therefore, we choose the single dataset [41] for detailed comparison. The non-monotonic oscillating behavior of the cross-sections in reactions R1, R2, and R3 was discussed in the original experimental papers and in Ref. [63]. Therefore, we do not discuss this behavior here.

Figure 4(d) shows that the datasets [45, 46, 64] for reaction R4 do not contradict to each other. Below, we compare with the calculations the combined dataset [46] at lower energies and [45] at higher energies. Finally, for reaction R5, we see in Fig. 4(e) that data from [48] do not agree with data from [47, 65]. However, there are only three overlapping points at above barrier energies from [47, 65]. Thus, we select data from [48] and [47] for separate detailed comparison with calculations. We omit data from [66] because there are only three suitable points with large errors.

For the selected experimental datasets, we perform a quantitative comparison between the theory and experiment using the conventional χ^2 criterion:

$$\chi^2 = \frac{1}{\upsilon} \sum_{i=1}^{\upsilon} \left(\frac{\sigma_{i\rm TM} - \sigma_{i\rm exp}}{\Delta\sigma_{i\rm exp}} \right)^2. \tag{21}$$

It is difficult to decide which collision energies to use from the experimental dataset for detailed quantitative comparison with calculations. In [13, 14] the criterion $\sigma_{\rm exp} > 200$ mb was chosen following Ref. [32]; this ap-

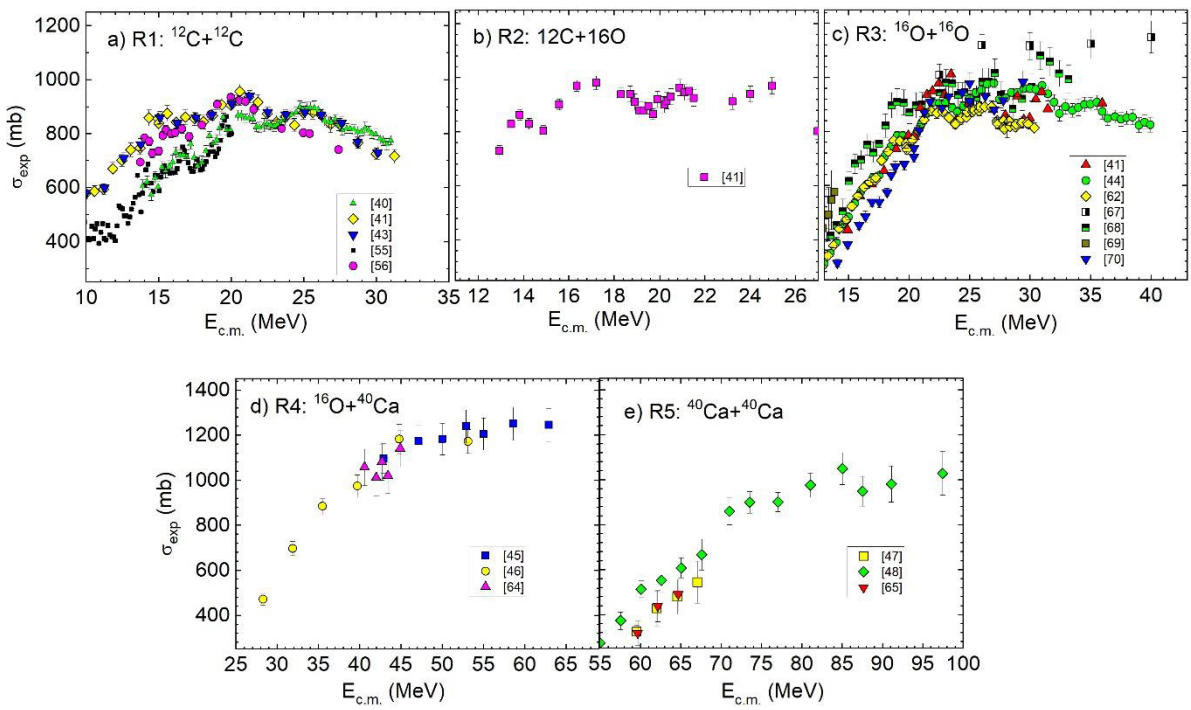

Fig. 4. (color online) Experimental fusion cross section versus the center-of-mass energy. References to the original papers are indicated in the panels. In many cases, data are taken from [61].

proximately corresponds to $E_{\rm c.m.} > 1.1B_0$. This criterion was formulated in [32] based on the coupled-channel calculations for the ^{16}O + ^{154}Sm reaction. Accordingly, in [13, 14], reactions were considered in which one of the colliding nuclei was ^{92}Zr or heavier. For such relatively heavy nuclei, the energies of the lowest excited states are at most 1 MeV, and the barrier energies are approximately 40 MeV or larger. Considering collisions at energies larger than $1.1B_0$, we can safely deal with the case in which several excited states are occupied at the barrier configuration, providing dissipation, which is an essential element of the TM.

In this study, collisions of light nuclei are considered, with the energy of first excited state being as large as 5 MeV and the barrier energy as low as 10 MeV. Therefore, even at $E_{\rm c.m.} \approx 2B_0$, we are not in the situation where several excited states are occupied, providing dissipation, at the barrier configuration. Therefore, in this study, we apply the phenomenological criterion $E_{\rm c.m.} > E_{\rm cut} = B_0 + E_2$, where E_2 is the lowest energy of the second excited state of two colliding nuclei.

The results of the TM-calculations depend on the friction strength K_R, for which the following empirical formula was obtained in [14]:

$$K_{Re} = K_1 \exp\left(\frac{B_0 - B_Z}{\Delta B}\right) + K_0. \tag{22}$$

Here,

$$B_Z = \frac{Z_1 Z_2}{A_1^{1/3} + A_2^{1/3}} \text{MeV} \tag{23}$$

is the approximate Coulomb barrier energy.

For the reactions ^{12}C+^{12}C, ^{12}C+^{16}O, and ^{16}O+^{16}O, Eq. (22) with the coefficients of [14] $K_1 = 260$ zs·GeV^{-1}, $K_0 = 10$ zs·GeV^{-1}, $B_0 = 7$ MeV, and $\Delta B = 15$ MeV results in $K_{Re} \approx 190 \div 260$ zs·GeV^{-1}. In the present calculations, these values lead to unrealistically small cross sections $\sigma_{\rm TM}$. Yet, Eq. (22) and its coefficients are based on the cross sections calculated for reactions with $B_Z > 40$ MeV, whereas for some reactions considered in this study, $B_Z < 13$ MeV. Therefore, we use the asymptotic value $K_R = K_0 = 10$ zs·GeV^{-1} as the first approximation and then vary K_R (if possible) to attempt to reach an agreement with the data.

In Fig. 5, we compare the calculated cross sections with the experimental values from Ref. [41] for reaction R1 and from Ref. [44] for reaction R3. The cross sections calculated using the BPM, $\sigma_{\rm BPM}$, significantly overshoot the experimental data at above barrier collision energies. We consider this an indication that friction is important in the process at these energies. It should be noted that the relation $\sigma_{\rm BPM} > \sigma_{\rm exp}$ holds for all considered reactions. The corss sections calculated accounting for dissipation, $\sigma_{\rm TM}$, agree with the measured values considerably better provided the value of K_R is chosen properly.

Such pictures are typical for other reactions and datasets; therefore, we prefer to present the ratios $\sigma_{\rm BPM}/\sigma_{\rm exp}$

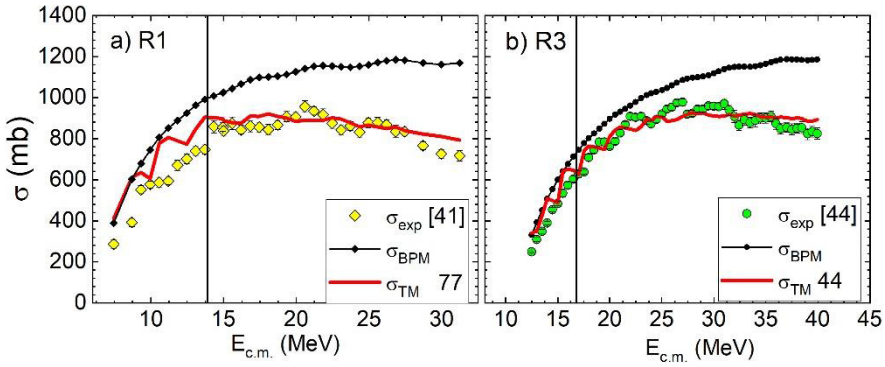

Fig. 5. (color online) For two reactions, theoretical fusion cross sections ($\sigma_{\rm BPM}$, lines with symbols; $\sigma_{\rm TM}$, lines without symbols) are compared with the experimental values (scatter symbols). The digits next to $\sigma_{\rm TM}$ are the values of $K_R/$ (zs$\cdot$GeV^{-1}) (see Table 2). The vertical lines correspond to $E_{\rm cut}$.

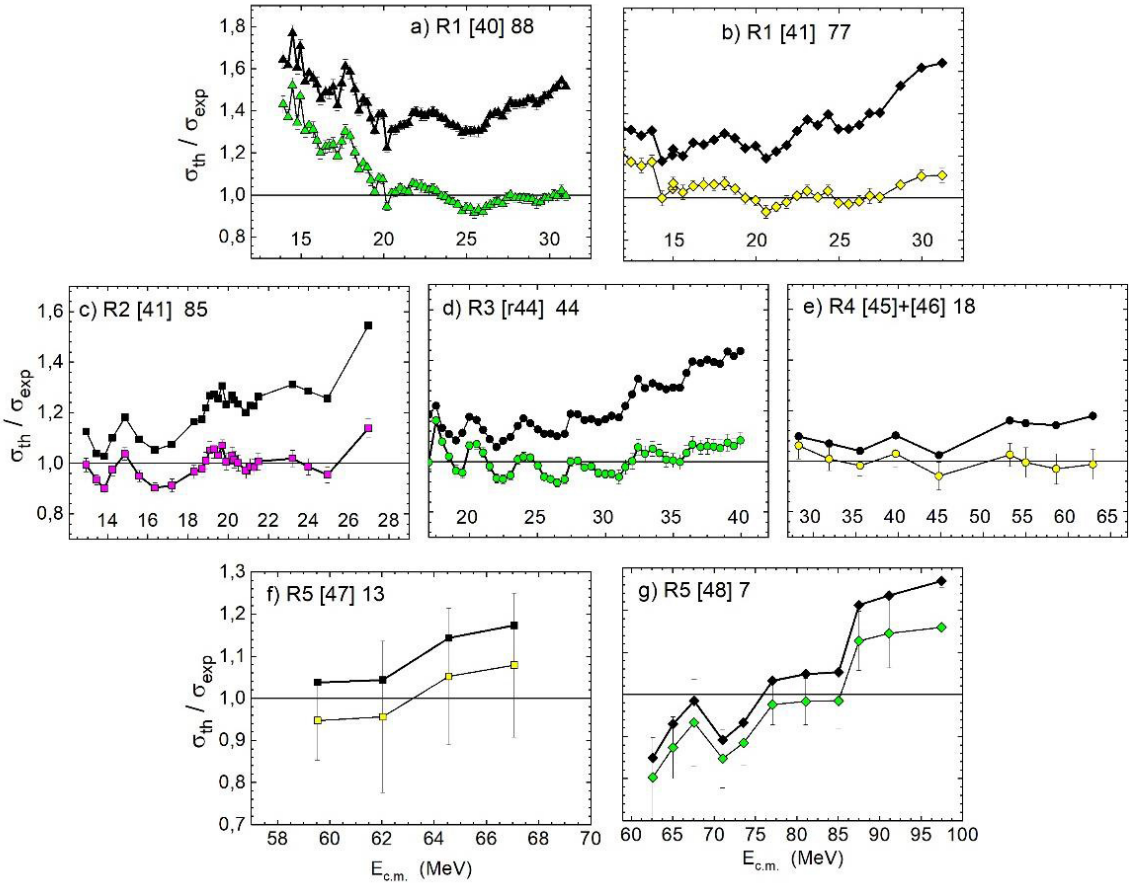

Fig. 6. (color online) Ratios $\sigma_{\rm BPM}/\sigma_{\rm exp}$ (upper curves) and $\sigma_{\rm TM}/\sigma_{\rm exp}$ (lower curves) versus collision energy for seven sets of data selected for detailed quantitative comparison. In each panel, the reaction number, the source of experimental data, and the values of $K_{Rm}/$(zs$\cdot$GeV^{-1}) are indicated.

and $\sigma_{\rm TM}/\sigma_{\rm exp}$ in Fig. 6. The values of $\sigma_{\rm TM}$ in these figures correspond to the values of K_R (K_{Rm}) providing the minimum value of χ^2 (χ^2_m). The values of K_{Rm} and χ^2_m and the number of data points involved in the χ^2-analysis, υ, are displayed in Table 2.

The quantitative results of the comparison between the TM and experiment are shown in Table 2. The TM provides a good description of the data. Note that at $K_R < 5$ zs$\cdot$GeV^{-1}, the resulting TM cross section becomes insensitive to the value of K_R, and $\sigma_{\rm TM}$ becomes close to $\sigma_{\rm BPM}$.

In Fig. 7, we show the values of K_{Rm} providing the best fit of the experimental fusion cross sections. The triangles represent the values of K_{Rm} obtained in Ref. [14].

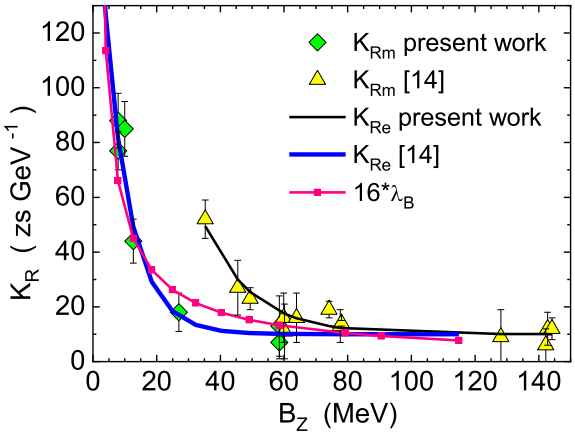

Fig. 7. (color online) Values of K_{Rm} obtained in [14] (triangles) and in the present study (diamonds). The lines indicate the approximations using Eq. (22) and the de Broglie wavelength multiplied by 16.

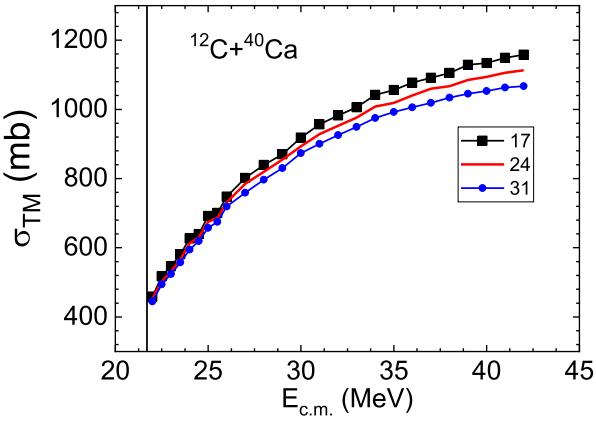

Fig. 8. (color online) Predicted fusion cross sections for the reaction ^{12}C+^{40}Ca calculated using the three values of K_R indicated in the figure. The vertical line corresponds to $E_{\rm cut}$.

In that study, the reactions with $B_Z > 40$ MeV were studied, and Eq. (22) was found to fit the values of K_{Rm} with a relative difference equal to 9.0% (this fit is shown in Fig. 7 by a thin black line).

Now, we have seven more values of K_{Rm} between 7 and 88 zs$\cdot$GeV^{-1} for $B_Z < 60$ MeV (diamonds in Fig. 7). The new set of K_{Rm} does not overlap with those from Ref. [14] except the heaviest reaction R5, ^{40}Ca+^{40}Ca. The values of K_{Rm} obtained in the present study are well approximated by Eq. (22) with the following set of coefficients: $K_1 = 80$ zs$\cdot$GeV^{-1}, $K_0 = 10$ zs$\cdot$GeV^{-1}, $B_0 = 7$ MeV, and $\Delta B = 8$ MeV (thick blue line in Fig. 7). Although the two curves for K_{Re} noticeably differ, the trend found in [14] holds: the smaller the B_Z, the larger the K_{Rm}. The physical meaning of this trend is still unclear.

We may consider a similarity between the behavior of $K_{Rm}(B_Z)$ and the de Broglie wavelength $\lambda_B(E_{\rm c.m.})$ for the imaginary particle with reduced mass, for which Eqs. (18) and (19) are written. We calculate $\lambda_B(E_{\rm c.m.})$ assuming $Z_1 = Z_2$, $A_1 = 2Z_1 = A_2 = 2Z_2$, and (somewhat arbitrarily) $E_{\rm c.m.} = B_Z$. The resulting dependence of $16\lambda_B(B_Z)$ is shown in Fig. 7 by a pink curve with small boxes. It reproduces the values of $K_{Rm}(B_Z)$ found in this study amazingly well and suggests a way for understanding the physical reason of the $K_{Rm}(B_Z)$-dependence.

Approximation (22) allows us to predict the value K_{Rm}=24 zs$\cdot$GeV^{-1} for the reaction ^{12}C+^{40}Ca, which is missing in Table 2 because we did not manage to find the corresponding experimental data. Accepting the uncertainty of the predicted K_{Rm} to be 7 zs$\cdot$GeV^{-1}, we obtain the cross sections shown in Fig. 8.

VI. SUMMARY

One of the methods widely used to obtain the nucleus-nucleus potential is the semi-microscopical double-folding model. Proton and neutron densities are important components of such a model. The adequate ND should not only provide good a nucleus-nucleus potential but also reproduce the experimental NCD.

In this study, we aim to achieve a good description of both the NCD and above-barrier fusion cross sections of even-even spherical light nuclei with $Z = N$: ^{12}C, ^{16}O, and ^{40}Ca. For this goal, we propose an approximation for the ND of these nuclei. This approximation, abbreviated as FE-density, provides a good description of the experimental NCDs.

Then, we use the FE NDs to evaluate the nucleus-nucleus potential via the double-folding model with density dependent M3Y-Paris *NN*-forces. Next, these potentials are applied to calculate the above-barrier fusion cross sections of the reactions ^{12}C+^{12}C, ^{12}C+^{16}O, ^{16}O+^{16}O, ^{16}O+^{40}Ca, and ^{40}Ca+^{40}Ca, where the experimental data are available. The cross sections are computed within two approaches: a) the BPM $\sigma_{\rm BPM}$ and b) the dynamical TM $\sigma_{\rm TM}$. In the latter case, the transmission coefficients are found using Langevin-type equations.

For all considered reactions, $\sigma_{\rm BPM}$ always exceeds $\sigma_{\rm exp}$. We believe this is a hint that at above-barrier energies, dissipation plays a significant role in collision process, thus requiring a dynamical model [32]. Our trajectory model reproduces the above-barrier experimental cross sections within 10%–15%. The only adjustable parameter of this model, the optimal friction strength K_{Rm}, is found to be approximately 90 zs$\cdot$GeV^{-1} for the light reactions ^{12}C+^{12}C, ^{12}C+^{16}O, and ^{16}O+^{16}O and approximately 15 zs$\cdot$GeV^{-1} for the heavier reactions ^{16}O+^{40}Ca and ^{40}Ca+^{40}Ca. This result does not strongly contradict the systematics found previously in Ref. [14]. Next, we readjust the coefficients of Eq. (22) to build the approximation for the values of friction strength obtained in the present study. Finally, we predict the value of K_{Rm} and calculate the cross sections $\sigma_{\rm TM}$ of the ^{12}C+^{40}Ca reaction, for which the experimental data seems to be miss-

ing.

Our FE-algorithm can be applied for above-barrier collisions of non-spherical nuclei with $Z = N$, such as ^{14}N, ^{22}Na, ^{32}S, because it is well known that nuclear deformations do not influence the above-barrier cross sections [32]. We plan to explore this possibility in the near future.

References

[1] A. S. Umar and V. E. Oberacker, Phys. Rev. C **73**, 054607 (2006)

[2] P.-G. Reinhard, A. S. Umar, P. D. Stevenson, Phys. Rev. C **93**, 044618 (2016)

[3] C. Simenel and A. S. Umar, Prog Part Nucl Phys. **103**, 19 (2018)

[4] G. Scamps and D. Lacroix, EPJ Web Conf **86**, 00042 (2015)

[5] V. V. Sargsyan, S. Yu. Grigoryev, G. G. Adamian *et al.*, Comp. Phys. Commun. **233**, 145 (2018)

[6] Yu. V. Palchikov, Z. Kanokov, G. G. Adamian *et al.*, Phys. Rev. E **71**, 016122 (2005)

[7] R. A. Kuzyakin, V. V. Sargsyan, G. G. Adamian *et al.*, Phys. Elem. Part. At. Nucl. , **48**, 21 (2017)

[8] G. G. Adamian, N. V. Antonenko, R. V. Jolos *et al.*, Int. J. Mod. Phys. E **5**, 191 (1996)

[9] M. Dasgupta, A. Navin, Y. K. Agarwal *et al.*, Nucl Phys. A **539**, 351 (1992)

[10] K. Hagino, N. Rowley, and A. T. Kruppa, Comp. Phys. Commun. **123**, 143 (1999)

[11] V. I. Zagrebaev and V. V. Samarin, Physics of Atomic Nuclei **67**, 1462 (2004)

[12] M. Dasgupta, D. J. Hinde, N. Rowley *et al.*, Ann. Rev. Nucl. Part. Sci. **48**, 401 (1998)

[13] I. I. Gontchar, R. Bhattacharya, and M. V. Chushnyakova, Phys. Rev. C **89**, 034601 (2014)

[14] M. V. Chushnyakova, R. Bhattacharya, and I. I. Gontchar, Phys. Rev. C **90**, 017603 (2014)

[15] M. V. Chushnyakova, I. I. Gontchar, and N. A. Khmyrova, Journal of Physics G:Nuclear and Particle Physics **48**, 015101 (2021)

[16] M. V. Chushnyakova, M. Bhuyan, I. I. Gontchar *et al.*, Nucl. Phys. A **994**, 121657 (2020)

[17] I. I. Gontchar and M. V. Chushnyakova, Journal of Physics G: Nuclear and Particle Physics **43**, 045111 (2016)

[18] V. Zagrebaev, A. Karpov, Y. Aritomo *et al.*, Physics of Particles and Nuclei **38**, 469 (2007)

[19] R. A. Kuzyakin, V. V. Sargsyan, G. G. Adamian *et al.*, Phys. Rev. C **85**, 034612 (2012)

[20] G. R. Satchler and W. G. Love, Phys. Rep. **55**, 183 (1979)

[21] D. T. Khoa, Phys. Rev. C **63**, 034007 (2001)

[22] I. I. Gontchar and M. V. Chushnyakova, Physics of Atomic Nuclei **79**, 543 (2016)

[23] S. Abrahamyan *et al.* (PREX Collaboration), Phys. Rev. Lett **108**, 112502 (2012)

[24] J. Yang, J. A. Hernandez, and J. Piekarewicz, Phys. Rev. C **100**, 054301 (2019)

[25] R. Hofstadter, F. Bumiller, and M. R. Yearian, Rev. Mod Phys. **30**, 482 (1958)

[26] H. de Vries, C. W. de Jager, and C. de Vries, At. Data Nucl. Data Tables **36**, 495 (1987)

[27] I. Angeli, At. Data Nucl. Data Tables **87**, 185 (2004)

[28] V. Yu. Denisov, N. A. Pilipenko, Fusion of deformed nuclei:12C+12C, Phys. Rev. C **81**, 025805 (2010)

[29] M. Yasue, T. Tanabe, F. Soga *et al.*, Nucl. Phys. A **394**, 29 (1983)

[30] Ahmed Hammad Amer, Zakaria M. M. Mahmoud, Yu. E., Nucl. Phys. A **1020**, 122398 (2022)

[31] D. T. Khoa, G. R. Satchler, and W. von Oertzen, Phys. Rev. C **56**, 954 (1997)

[32] J. O. Newton, R. D. Butt, M. Dasgupta *et al.*, Phys. Rev. C **70**, 024605 (2004)

[33] Z. Łojewski, B. Nerlo-Pomorska, K. Pomorski *et al.*, Phys. Rev. C **51**, 601 (1995)

[34] J.-L. Basdevant, J. Rich, and M. Spiro, *Fundamentals in Nuclear Physics: From Nuclear Structure to Cosmology* (Springer Science & Business Media, 2005)

[35] R. Pohl *et al.*, The Size of the Proton, Nature **466**, 213 (2010)

[36] N. Bezginov, T. Valdez, M. Horbatsch *et al.*, Science **365**-1007 (1979)

[37] R. Capote, M. Herman, P. Obložinský *et al.*, Nucl. Data Sheets **110**, 3107 (2009)

[38] I. I. Gontchar, D. J. Hinde, M. Dasgupta *et al.*, Phys. Rev. C **69**, 024610 (2004)

[39] P. Fröbrich and R. Lipperheide, *Theory of Nuclear Reactions* (Clarendon Press, Oxford, 1996).

[40] J. J. Kolata, R. M. Freeman, F. Haas *et al.*, Phys. Rev. C **21**, 579 (1980)

[41] D. G. Kovar, D. F. Geesaman, T. H. Braid *et al.*, Phys. Rev. C **20**, 1305 (1979)

[42] M. N. Namboodiri, E. T. Chulick, and J. B. Natowitz, The Fusion of 12C with 12C at Projectile Energies from 45 to 197 MeV, Nuclear Physics, Section A **263**, (1976).

[43] P. Sperr, T. H. Braid, Y. Eisen *et al.*, Phys. Rev. Lett **37**, 321 (1976)

[44] J. J. Kolata, R. M. Freeman, F. Haas *et al.*, Phys. Rev. C **19**, 2237 (1979)

[45] Y. Nagashima, J. Schimizu, T. Nakagawa *et al.*, Phys. Rev. C **33**, 176 (1986)

[46] S. E. Vigdor, D. G. Kovar, P. Sperr *et al.*, Phys. Rev. C **20**, 2147 (1979)

[47] H. A. Aljuwair, R. J. Ledoux, M. Beckerman *et al.*, Phys. Rev. C **30**, 1223 (1984)

[48] H. Doubre, A. Camp, J. C. Jacmart *et al.*, Phys. Lett. B **73**, 135 (1978)

[49] M. V. Chushnyakova and I. I. Gontchar, Phys. Rev. C **87**, 014614 (2013)

[50] P. Fröbrich, Phys. Rep. **116**, 337 (1984)

[51] K. Wen, F. Sakata, Z.-X. Li *et al.*, Phys. Rev. Lett. **111**, 012501 (2013)

[52] D. H. E. Gross and H. Kalinowski, Phys. Rep. **45**, 175 (1978)

[53] A. E. Gegechkori, Y. A. Anischenko, P. N. Nadtochy *et al.*, Physics of Atomic Nuclei **71**, 2007 (2008)

[54] M. V. Chushnyakova and I. I. Gontchar, Journal of Physics G **40**, 095108 (2013)

[55] L. J. Satkowiak, P. A. DeYoung, J. J. Kolata *et al.*, Phys. Rev. C **26**, 2027 (1982)

[56] M. Conjeaud, S. Gary, S. Harar *et al*., Nucl. Phys. A **309**, 515 (1978)
[57] E. F. Aguilera *et al*., Phys. Rev. C **73**, 064601 (2006)
[58] B. Dasmahapatra, B. Čujec, and F. Lahlou, Nuclear Physics, Section A **384** (1982)
[59] M. D. High and B. Čujec, Nucl Phys. A **282**, 181 (1977)
[60] R. L. Parks, S. T. Thornton, L. C. Dennis *et al*., Nucl Phys. A **348** (1980)
[61] V. I. Zagrebaev, A. S. Denikin, A. V. Karpov *et al*., Nuclear Instruments and Methods in Physics Research **859**, 112 (2017)
[62] J. J. Kolata, R. C. Fuller, R. M. Freeman *et al*., Phys. Rev. C **16**, 891 (1977)
[63] M. V. Chushnyakova and I. I. Gontchar, Pramana **85**, 653 (2015)
[64] D. F. Geesaman, C. N. Davids, W. Henning *et al*., Phys. Rev. C **18**, 284 (1978)
[65] G. Montagnoli, A. M. Stefanini, C. L. Jiang *et al*., Phys. Rev. C **85**, 024607 (2012)
[66] E. Tomasi, D. Ardouin, J. Barreto *et al*., Nucl. Phys. A **373**, 341 (1982)